Clays and Clay Minerals, Vol. 58, No. 6, 727–742, 2010.

AUTOMATED FITTING OF X-RAY POWDER DIFFRACTION PATTERNS FROM INTERSTRATIFIED PHYLLOSILICATES

HONGJI YUAN[1,*] AND DAVID L. BISH[1]

[1] Department of Geological Sciences, Indiana University, Bloomington, IN 47405 USA

Abstract—NEWMOD©, developed by R.C. Reynolds, Jr., has been an important tool for evaluating quantitatively X-ray diffraction (XRD) patterns from interstratified clay minerals for more than 20 years. However, a significant drawback to the NEWMOD© approach is that analyses are done by forward simulation, making results sensitive to user input and starting-model assumptions. In the present study, a reverse-fitting procedure was implemented in a new program, FITMOD, which automatically minimizes the differences between experimental and simulated XRD patterns. The differences are minimized by varying model parameters (such as Reichweite, crystal-size distribution, cation content, type of disorder, *etc*.) using the downhill simplex method. The downhill simplex method is a non-linear optimization technique for determining minima of functions. This method does not require calculation of the derivatives of the functions being minimized, an important consideration with many of the parameters in NEWMOD-type simulations. Instead, the downhill simplex method calculates pseudo-derivatives by evaluating sufficient points to define a derivative for each independent variable. The performance of FITMOD was evaluated by fitting a series of synthetic XRD patterns generated by NEWMOD+, yielding agreement factors, R_{wp}, of <0.3%. As long as the correct interstratified system was specified (*e.g.* illite-smectite), excellent fits were obtained irrespective of the starting parameters for the simulations. FITMOD was also tested using experimental XRD patterns, which gave very good fits, in agreement with previously published results. The optimization routine yields good fits for both synthetic and experimental XRD profiles in a reasonable time, with the possibility of varying all important structural parameters. FITMOD automatically provides optimum fits to experimental XRD data without operator bias, and fitting efficiency and accuracy were, therefore, significantly improved.

Key Words—Downhill Simplex, FITMOD, Fitting, Least Squares, NEWMOD+, X-ray Diffraction.

INTRODUCTION

Interstratification in phyllosilicates has been an important aspect of clay mineralogy since it was first reported by Gruner (1934). Distinct from a physical mixture, different interstratified component layers stack along the *Z* direction to create a domain that diffracts more or less coherently. Depending on the ordering of stacking, interstratification can be categorized in one of three ways: ordered, random, or partially ordered (Reynolds, 1980). Ordered interstratification results in a supercell along the *Z* direction, and diffraction occurs from repeats (d_{001}) equal to the sum of the thicknesses of each individual layer within the superstructure. For instance, an ordered alternating sequence of talc and chlorite, the basal spacings of which are 9.4 Å and 14 Å, respectively, produces a repeat in the *Z* direction of 23.4 Å and has been named kulkeite (Schreyer *et al.*, 1982). Unlike single phyllosilicate phases or ordered interstratifications, randomly interstratified materials exhibit an irrational series of basal reflections that imperfectly satisfy the Bragg equation, $n\lambda = 2d \sin\theta$. The degree to which irrational basal reflections depart from the Bragg condition is a sensitive indication of interstratification and is controlled by the ordering and proportions of interstratified components, component repeat differences along Z, and departures from rationality. Since interstratification was first recognized, important contributions have been made by Hendricks and Teller (1942), Méring (1949), MacEwan (1958), MacEwan *et al.* (1961), Reynolds (1967), Drits and Sakharov (1976), Plançon (1981), Bethke and Reynolds (1986), and Drits *et al.* (1997a). Reynolds (1980) reviewed the history of analysis of interstratified phyllosilicates by XRD, and the details will not be repeated here.

NEWMOD© was developed specifically for the study of two-component interstratifications of clay minerals (Reynolds, 1985). The program can generate simulated XRD patterns, given the proportions of the two clay mineral components and the state of ordering (Walker, 1993). Investigators have been able to extract structure information by fitting experimental data with a calculated pattern by manually modifying input parameters. Structure information includes component proportions, ordering state (Reichweite value), as well as crystallite size and size distribution. These parameters are difficult or impossible to obtain using other analytical methods. As a result, NEWMOD© has been used widely in the

* E-mail address of corresponding author:
honyuan@indiana.edu
DOI: 10.1346/CCMN.2010.0580601

https://doi.org/10.1346/CCMN.2010.0580601 Published online by Cambridge University Press

study of interstratified clay minerals (*e.g.* Wilson *et al.*, 1992; Hillier and Velde, 1992; Berkgaut *et al.*, 1994; Renac and Meunier, 1995; Jaboyedoff and Thelin, 1996; Drits *et al*., 1997a, 1997b; Jaboyedoff and Cosca, 1999; de la Fuente *et al.*, 2002; Cuadros and Dudek, 2006; Dudek *et al.*, 2006; Gualtieri *et al.*, 2008) and is one of the primary tools for interpreting XRD patterns of such materials.

In addition to NEWMOD©, the program developed by Drits and Sakharov (1976) was recently modified to interpret more complicated cases involving multiple interstratifications of multiple components (Drits *et al.*, 1997b). The program DIFFaX (Treacy *et al.*, 1991) uses a general recursive method to simulate diffraction effects from any crystal having planar defects. The application of DIFFaX in clay mineralogy, however, has been limited in practice because it requires the user to define the complete stacking sequence, including translational (and rotational) vectors and the stacking transition probability matrix. Parametric refinement of DIFFaX has been implemented in two extensions, namely DIFFaX+ (Leoni *et al.*, 2004) and FAULTS (Casas-Cabanas *et al.*, 2005). DIFFaX+ allows refinement of crystal structure and microstructure simultaneously. However, the potential and stability of both programs when applied to complex structures (*e.g.* clay minerals) have been questioned (Gualtieri *et al.*, 2008). Recently, Ufer *et al.* (2008) modified the Rietveld code, BGMN (Bergmann *et al.*, 1994), by incorporating the recursive method used in DIFFaX. Their modified version of BGMN allows simulation of diffraction patterns of layered materials with stacking defects and it allows simultaneous refinement of both disorder and structure parameters. The DISCUS program (Proffen and Neder, 1997) provides a more general way to model the effects of defects (atomic, dislocation, and vacancies) and finite crystallite size/shape by constructing a super cell containing a large number of elementary unit cells. Refinement of structural parameters can be conducted using the refinement routine DIFFEV. The DISCUS program has generally been used to model highly defective nano-materials with simple chemical compositions.

In contrast to other least-squares crystallographic-fitting applications, such as the Rietveld method, a trial-and-error method has been used widely in fitting XRD patterns of interstratified layered materials. This approach has significant limits as it requires intense interaction between the program (*e.g.* NEWMOD©) and investigator and is, therefore, time consuming and tedious. Moreover, the resulting fit is usually a semi-quantitative match that is generally user dependent. The profile fitting (matching) methodology used in NEWMOD© relies purely on a trial-and-error method, and the revised program of Drits and Sakharov (1976) also employs this method to determine the structural, chemical, and ordering probability parameters for each interstratified phase (Drits *et al.*, 2002). Although the drawbacks of the trial-and-error approach are well known, analysis of interstratified materials has not yet advanced to an 'inverse modeling' approach that would facilitate improvement in the efficiency and accuracy of profile fitting. The combination of probability parameters that describe ordering of interstratified components and integer parameters (*e.g.* coherent-scattering-domain (CSD) size and minimum and maximum size distribution) makes the automatic fitting of profiles difficult when using common minimization techniques that rely on function gradient (such as the method used in the Rietveld method). Drits *et al.* (2002) reduced user interaction and bias by employing numerical minimization techniques to determine the fractions of different interstratified phases. However, their method uses compositions and ordering parameters that were pre-selected by trial-and-error methods. Importantly, in this case, user bias was already established during the compositional and ordering parameter determination process, and hence the application of numerical minimization does not improve the accuracy. On the other hand, the application of a genetic algorithm (GA) using NEWMOD© by Pevear and Schuette (1993) in the program MatchMod can be considered the only approach to date that fundamentally reduces user bias. All adjustable parameters are varied by the optimization routine (the GA), but several problems can arise during the application of a GA with the NEWMOD© architecture. First, the algorithm lacks a convergence mechanism and, consequently, the program may continue for hours without significant improvement in the result. Second, continuous parameters are split into discrete values and a good fit result cannot be achieved if the parameters were not split sufficiently finely. However, the finer the segment size, the greater the calculation time. As the number of adjustable parameters increases, the application of a GA to profile fitting of interstratified systems becomes impractical without introducing a parallel computing methodology.

The application of a forward minimization algorithm based on the downhill simplex method to automate profile fitting of measured XRD patterns of interstratified clay minerals based on the NEWMOD© architecture is presented here. The method is distinct from all previous methods, including the GA method. The downhill simplex method is a non-linear optimization technique for determining minima of functions. Unlike minimization methods used in traditional crystal-structure refinement (*e.g.* Levenberg-Marquardt or Gauss-Newton), the downhill simplex method requires no calculation of the derivatives of the functions being minimized, which is an important consideration with many of the parameters in NEWMOD-type simulations. Instead, the downhill simplex method calculates pseudo-derivatives by evaluating sufficient points to effectively define a derivative for each independent variable.

https://doi.org/10.1346/CCMN.2010.0580601 Published online by Cambridge University Press

METHODS

NEWMOD+

The NEWMOD© program developed by Reynolds (1985) suffers from several drawbacks related to structural models and inconvenient operation. Yuan and Bish (2010) developed a new program, NEWMOD+, loosely based on NEWMOD©. This program incorporates recent progress on mineral structures (Ferrage *et al.*, 2005a, 2005b) and greatly improves the fitting efficiency and accuracy within an integrated simulation environment. The program also presents convenient graphical comparisons as well as numerical quantities to describe fit quality.

Modeling the ordering of interstratified components in the NEWMOD approach involves a set of probability parameters, *e.g.* PA, PBA, PBAA, and PBAAA (PA = probability of A, PBA = probability of an A, given a B, *etc.*). The probability parameters (PA, PBA, PBAA, and PBAAA) are correlated and, therefore, only some combinations of these parameters can lead to a sensible ordering scheme. Therefore, parameters can vary only over a limited range to produce a meaningful result. NEWMOD© does not explicitly limit the possible range for each of the probability parameters and, consequently, the user can encounter difficulty in optimizing these transition-probability parameters. The general assumption is that the Reichweite value is an integer used to quantitatively describe an observed diffraction pattern, but the Reichweite value can have non-integer values. Indeed, Reynolds (1985) combined the Reichweite value with the probability parameters, *e.g.* PBA, PBAA, *etc.*, to describe interstratification order in NEWMOD© in which Reichweite application was extended to non-integer values, namely 0.5, 1.5, and 2.5. As a random interstratification is ultimately based on a probabilistic representation of the component layers, integer values of Reichweite are merely a simplification. Assuming that no long sequences of B (the minor component) layers exist, *i.e.* the probability of occurrence of B depends only on the preceding layer, the three transition probability parameters PBA, PBAA, and PBAAA can be calculated given only a pair of PA and Reichweite values (see Reynolds, 1980, p. 255). The Reichweite value is treated in NEWMOD+ as a continuous variable. Thus, the user can adjust the three transition probability parameters simultaneously simply by changing the Reichweite value, thereby greatly improving the fitting efficiency and accuracy. Moreover, replacement of the three transition-probability parameters with one numerical value for Reichweite facilitates automated fitting using numerical optimization. Reducing the number of fitting parameters from three (PBA, PBAA, and PBAAAA) to one (Reichweite) minimizes the complexity of changing boundary conditions during the optimization process.

Isomorphic substitutions in the tetrahedral and octahedral sheets and heterogeneity in the interlayer (*e.g.* different cations and H_2O molecules at different sites) result in finite thickness variations of individual layers (*i.e.* basal spacing). The accumulated effects of such variations were termed first-type or second-type disorder by Guinier (1964). The effects of both of these on X-ray diffraction (XRD) profiles were discussed in detail by Reynolds (1989) and Drits and Tchoubar (1990), in which a first-type defect was treated as a thermal effect. The second-type disorder was treated as strain, which broadens peaks and lowers the intensities (only 00*l* reflections, one-dimensional). Modeling first-type and second-type disorder can be accomplished by assuming that basal-spacing fluctuations follow a Gaussian distribution (Drits *et al.*, 2005). Two parameters (ε_I and ε_{II}) are required to describe apparent basal spacing deviations for each layer component. Hence, four additional disorder parameters (ε_I and ε_{II}) for each component were required to simulate the two-component interstratified system implemented in NEWMOD+.

Numerical optimization and profile-fitting methods

The numerical optimization routine developed in FITMOD is a significant extension of NEWMOD+ as it permits automated fitting of experimental diffraction profiles. Numerous synthetic and experimental XRD profiles were examined using FITMOD. The ultimate profile-fitting goal is to obtain a best fit to an observed profile by optimizing adjustable parameter values in the model, thereby simulating a one-dimensional diffraction pattern. The goodness of fit can be defined by equation 1:

$$R = \sum_{i=1}^{N} (y_{oi} - y_{ci}) \quad (1)$$

in which R, the agreement factor or total residual error, is related to the sum of the discrepancies, on a point by point basis, between y_c, the calculated profile, and y_o, the observed profile, over the entire diffraction range. A well distributed error tends to yield a value of zero for R because positive and negative terms cancel. In order to avoid cancelation of errors, two different schemes have commonly been applied (Young, 1993), given by equations 2 and 3:

$$R = \sum_{i=1}^{N} |y_{oi} - y_{ci}| \quad (2)$$

$$R = \sum_{i=1}^{N} (y_{oi} - y_{ci})^2 \quad (3)$$

A general method for optimization is based on the fact that changes in total residual error, ΔR, equal zero when R reaches a minimum and thus the partial derivatives, $(dR)_{a_j}$, with respect to each adjustable parameter, a_j, in the model equal zero. Such an approach was represented by the Levenberg-Marquardt algorithm (Marquardt, 1963) and is commonly used in powder diffraction-profile fitting

https://doi.org/10.1346/CCMN.2010.0580601 Published online by Cambridge University Press

(Howard and Preston, 1989). In contrast to this approach requiring the calculation of derivatives at each point, the downhill simplex method (Nelder and Mead, 1965) does not require calculation of derivatives. Derivative-based methods converge much more quickly than Nelder's downhill simplex method, if the derivatives can be solved analytically (Howard and Snyder, 1983). However, application of the Levenberg-Marquardt method to the NEWMOD© model is problematic.

Close examination of the NEWMOD© model shows that it is non-linear. This non-linearity can be observed in the model intensity function (*i.e.* equation 11 in Reynolds, 1980) and also in the variable constraints, such as the partial dependence of Reichweite value on component properties. For example, the Reichweite value can vary only between 0 (random) and 1.25 when the major-component fraction, PA, is set to 0.6. Moreover, calculation of the frequency term, σ, in MacEwan's (1958) mixing function by the regression method renders the analytical calculation of most parameter derivatives impossible, with only several exceptions such as the scale factor (SF). The frequency term, σ, corresponds to the occurrence probability of layer sequences that are terminated by the same end layers and have identical spacings and compositions (Reynolds, 1980). Alternately, derivatives can be obtained by numerical approximation. However, numerical differentiation increases calculation time by up to an order of magnitude and is affected by truncation and round-off errors. Furthermore, numerical differentiation methods are inappropriate for calculating derivatives of the two integer adjustable parameters, HighN and LowN, which describe the minimum and maximum CSD size, respectively.

In contrast to the Levenberg-Marquardt method, Nelder's downhill simplex method requires no derivatives and instead calculates pseudo-derivatives by evaluating sufficient points to effectively define a derivative for each independent variable. This significant advantage makes it the optimization method of choice for fitting within the NEWMOD© architecture.

A brief introduction to Nelder's downhill simplex method would be useful here. Given M parameters to refine, Nelder's downhill simplex algorithm constructs an initial simplex with M+1 vertices and each vertex represents a vector (Press *et al.*, 1992; en.wikipedia.org/wiki/Nelder%E2%80%93Mead_method),

$$P_i = P_0 + \lambda e_i \tag{4}$$

where the e_i values are M unit vectors and λ is a constant that is the step size. Generally, e_i is set to unity, so the vectors are organized in the following way:

$$\begin{aligned} p_0 &= (x_0,x_1,x_2,\cdots x_M) \\ p_1 &= (x_0,x_1+\lambda,x_2,\cdots x_M) \\ p_2 &= (x_0,x_1,x_2+\lambda,\cdots x_M) \\ \cdots &= \cdots \\ p_n &= (x_0,x_1,x_2,\cdots x_M+\lambda) \end{aligned} \tag{5}$$

where each vector P_i is associated with the value of the evaluated function, which in the present case is the total residual error, R, with the parameter configured in vector P_i. Such a simplex (polytope, an n-dimensional geometrical object with flat sides) represents n-dimensional parameter space, and the downhill simplex method optimization progresses through a series of iterations. In a 'reflection' operation, each iteration reflects the largest R-value vertex, P_j, to the other side of the simplex through a reflection plane or the simplex center. In an 'expansion' operation, the residual is reduced and the vertex, P_j, is moved further along the same direction, which speeds convergence. The vertex, P_j, contracts toward the simplex center if the previous reflection operation failed to reduce the residual. The final operation, termed 'multiple contraction,' contracts all vertices until the residual is minimized. The downhill simplex method manipulates the simplex through these geometrical operations until certain termination criteria have been met. Several criteria are available for terminating the iteration. Iterations can be stopped either when the amplitude of geometrical operation, *i.e.* operation step size, is smaller than a preset tolerance value, or when the decrease in function values reaches a certain tolerance value. A maximum iteration number can be set as an additional termination criterion when the iteration converges extremely slowly. As with most optimization methods, the downhill simplex method yields a minimum without providing additional information concerning whether it has reached a *global* minimum. Consequently, an additional procedure is required to test the results and, more importantly, provide the downhill simplex method with the ability to climb out of a local minimum. This procedure involves perturbing a local minimum by taking a finite amplitude step away from it and then determining whether the refinement returns to a lower minimum or consistently returns to the same minimum state.

Criteria for assessment of fitting results

The total residual errors defined by equations 2 and 3 increase with the number of observed points. Consequently, the total residual errors must be normalized for the purpose of comparing the goodness of fit for different patterns. In accordance with the two different schemes for R, R was normalized with two different denominators given in equations 6 and 7:

$$R_{p1} = \sum_{i=1}^{N} |y_{oi} - y_{ci}| / \sum_{i}^{N} y_{oi} \tag{6}$$

$$R_{p2} = \left(\sum_{i=1}^{N} (y_{oi} - y_{ci})^2 / \sum_{i=1}^{N} y_{oi}^2 \right)^{1/2} \tag{7}$$

Equations 6 and 7 are termed unweighted profile residual errors (Howard and Preston, 1989), and each

https://doi.org/10.1346/CCMN.2010.0580601 Published online by Cambridge University Press

point is assumed to have the same error distribution. Thus, the errors contribute equally to the total residual error, R. These two unweighted fitting schemes have been used widely in crystallographic refinement methods, such as the Rietveld method and other optimization routines (Ferrage *et al.*, 2005a, 2005b). R_{p2} is the quantity typically used in least-squares refinements. The intensity measured by a detector at each data point through direct counting of quanta in X-ray diffractometry often deviates from the "true" value (Toby, 2006) which follows a Gaussian distribution when the measured intensity is high (>20 counts, David, 2004). To account for such deviations in measured intensities, a weighted profile residual error, R_{wp}, is calculated using a point-by-point weighting factor, w_i, applied to each term in the fitting scheme. The R_{wp} value, expected-R, goodness-of-fit χ^2 (chi-square), and other fitting criteria are favored in many crystallographic-optimization routines. The expressions used for these weighted fitting schemes were given by David (2004) as:

$$R_{wp} = \left[\left(\sum_{i=1}^{N} w_i (y_{oi} - y_{ci})^2 \right) / \sum_{i=1}^{N} w_i y_{oi}^2 \right]^{1/2} \quad (8)$$

$$R_{\text{exp}} = \left[(N - P + C) / \sum_{i=1}^{N} w_i y_{oi}^2 \right]^{1/2} \quad (9)$$

$$\chi^2 = (R_{wp}/R_{\text{exp}})^2 = \sum_{i=1}^{N} w_i (y_{oi} - y_{ci})^2 / (N - P + C) \quad (10)$$

where N is the number of observations, P is the number of variable parameters, and C indicates the number of constraints applied among adjustable parameters. The term y_{oi} is the observed intensity at point i, y_{ci} is the calculated intensity at point i (based on model), and w_i is the weighting factor. A value of $1/y_{oi}$ is commonly applied as a weighting factor, w_i, considering a Poisson error distribution. However, one should carefully consider the effect of applying $1/y_{oi}$ weighting because it accentuates the error contribution from the misfit where the intensity is low, whereas the contribution from misfit at high intensity (probably the tops of peaks) is greatly reduced. Therefore, the optimization process can potentially yield a diffraction profile that fits the portion of the XRD pattern with low intensity well and greatly differs from the fitting target (the observed data) for high-intensity portions. The choice of a specific fitting criterion thus depends strongly on the model as well as on the data being fitted.

In addition to these fitting criteria that serve as minimization goals in FITMOD, adjustable-parameter values obtained by profile-fitting synthetic patterns can be compared directly with preset values in fitting targets through equation 11

$$\text{Accuracy (\%)} = [1 - |P_{\text{target}} - P_{\text{fitting}}|/P_{\text{target}}] \times 100 \quad (11)$$

This simple and direct comparison of the values of fitting parameters can provide a means to evaluate the performance of an optimization routine in terms of fitting accuracy. More importantly, it facilitates improved understanding of the nature of the parameters, *e.g.* the effects of parameters on profile shapes and intensities and correlations among parameters. This information can then be used to improve confidence when fitting unknown experimental profiles. Because the accuracy of parameters determined from experimental profiles of real interstratified samples cannot be evaluated, fits to simulated patterns (calculated with known structural parameters using NEWMOD+) were performed to determine the influence of the adjustable parameters on the XRD profiles. The more influence on a profile (overall intensities) a particular parameter has, the more accurate will be the refined value. Fitting results obtained with simulated patterns suggested that parameters related to the thickness of individual components (d_{001} values), the fractional percentage of individual interstratified components, ordering, and sample orientation can be refined with high accuracy. In contrast, refined parameters relating to chemical composition, *i.e.* concentration of Fe, K, and interlayer species, did not agree as well with preset values, suggesting that further constraints during refinement are required, such as reducing boundary conditions during refinement or taking advantage of additional information (*e.g.* chemical analyses) in formulating refinement constraints.

RESULTS AND DISCUSSION

Evaluation of numerical optimization and profile fitting using synthetic profiles

The accuracy and precision of FITMOD was evaluated by fitting synthetic XRD patterns generated by NEWMOD+. These tests of the optimization routine incorporated as many adjustable parameters as possible, and different fitting criteria were evaluated, namely unweighted fitting schemes (R_{p1}, R_{p2}) *vs.* a weighted scheme (R_{wp}). Two interstratified systems, *i.e.* an interstratified one-H_2O layer-two-H_2O layer (1W-2W) smectite and an interstratified illite-smectite (I-S) solvated with ethylene glycol (EG), abbreviated as I-S(EG), were chosen as synthetic fitting targets, followed by comparison with similar experimental profiles.

Parameter values used (Tables 1 and 2) included those to generate the synthetic profile of interstratified 1W-2W smectite, all fixed parameters, and X-ray diffractometer and sample-mount characteristics. Note that initial values of parameters used in fitting were generally chosen to be different from the true values. Optimum parameter values (Table 1) were obtained

https://doi.org/10.1346/CCMN.2010.0580601 Published online by Cambridge University Press

Table 1. Values of fitting parameters used for fits to synthetic interstratified one-H_2O layer-two-H_2O layer (1W-2W) smectite.

Parameter	Target value	Initial value	LB	UB	R_{p1} Refined value	R_{p1} Accuracy	R_{p2} Refined value	R_{p2} Accuracy	R_{wp} Refined value	R_{wp} Accuracy
$P_{(2W)}$	0.77	0.6	0.5	1	0.77	100.0	0.77	100.0	0.77	100.0
$d_{001(2W)}$	15.30	15	15.1	15.8	15.31	99.9	15.30	100.0	15.30	100.0
$\varepsilon_{I(2W)}$	0.15	0.1	0	0.5	0.11	73.3	0.17	86.7	0.15	100.0
$\varepsilon_{II(2W)}$	0.30	0.1	0	0.5	0.33	90.0	0.30	100.0	0.30	100.0
$d_{001(1W)}$	12.50	12.4	12.3	12.7	12.49	99.9	12.50	100.0	12.50	100.0
$\varepsilon_{I(1W)}$	0.10	0.1	0	0.5	0.18	20.0	0.18	20.0	0.18	20.0
$\varepsilon_{II(1W)}$	0.25	0.1	0	0.5	0.19	76.0	0.22	88.0	0.25	100.0
Fe	0.80	0.5	0	1.7	0.73	91.3	0.84	95.0	0.80	100.0
CEC	0.36	0.3	0.25	0.6	0.51	58.3	0.25	69.4	0.48	66.7
C_{1W}	2.10	2	1	2.5	1.00	47.6	1.97	93.8	1.94	92.4
B_{1W}	11.00	2	0	25	13.15	80.5	12.30	88.2	2.51	22.8
C_{2W}	4.50	2.8	2.5	6	4.05	90.0	4.39	97.6	4.37	97.1
Δd_{wat}	1.40	1.2	1.1	1.6	1.37	97.9	1.31	93.6	1.43	97.9
B_{2W}	20.00	11	0	25	5.13	25.7	13.42	67.1	16.89	84.5
DFD	3.00	1.5	0	10	3.00	100.0	3.00	100.0	2.99	99.7
High N	25	14	4	50	24	96.0	24	96.0	25	100.0
Reichweite	1.50	1	0	3	1.53	98.0	1.50	100.0	1.50	100.0
Sigmastar	6.00	12	0	30	7.06	82.3	6.71	88.2	5.99	99.8
SF	1.50	6	0	1000	1.82	78.4	1.71	86.0	1.50	100.0

Target value: value used in calculating the synthetic profile; Initial value: parameter value used to begin the fit; LB, UB: lower boundary, upper boundary of the parameter in the optimization; $P_{(2W)}$: the fraction of component 2W smectite; $\varepsilon_{I(1W)}$, $\varepsilon_{II(1W)}$, $\varepsilon_{I(2W)}$, $\varepsilon_{II(2W)}$: first-type and second-type disorder in 1W and 2W smectite; C_{1W}, C_{2W}: concentration of interlayer H_2O in 1W and 2W smectite, respectively; B_{1W}, B_{2W}: thermal factor of interlayer H_2O in 1W and 2W smectite; Δd_{wat}: the position of interlayer H_2O away from mid-plane of interlayer region; DFD: defect-free distance; Sigmastar: quantity describing sample-preferred orientation; SF: scale factor.

using the different fitting criteria (R_{p1}, R_{p2}, and R_{wp}). Fitting-parameter accuracies were calculated using equation 11, and the optimized fits were plotted (Figure 1). Visual evaluation of results suggest that the weighted fitting scheme (R_{wp} = 0.29%) provided a better fit than unweighted fitting schemes (R_{p1} = 0.685% and R_{p2} = 0.16%). Note that all three R values were very small and reflect excellent fits. Although the R_{p2} value was smaller than the R_{wp} value, significant misfit in the 006 to 007 reflection region was observed (Figure 1b), which was optimized using R_{p2}. Misfits in the R_{p1}-optimized fit are also present in the 004 and 008 reflection regions. In contrast, the fit obtained using R_{wp} matches the fitting target well with no significant discrepancies. Misfits observed in the optimized profiles yielded by the unweighted fitting schemes are located in regions with relatively low intensity and arise from the nature of R_{p1} and R_{p2}, which focus on misfit in high-intensity regions by applying more weight to these discrepancies. On the other hand, R_{wp} does essentially the opposite by effectively accentuating the error contribution from misfit where the intensity is low and reducing the contribution from misfit at high intensities (the tops of peaks).

Table 2. Values of fixed parameters for interstratified one-H_2O layer-two-H_2O layer (1W-2W) smectite diffraction data.

Name	Value	Name	Value
Major component	Dismectite (2W)	Mustar (cm^2/g)	40
Minor component	Dismectite (1W)	Theta compensating slit	FALSE
λ (Å)	1.5406	RNDPWD	TRUE
Divergence slit (º)	0.5	2θ start (º)	2
Goniometer radius (cm)	21.75	2θ end (º)	50
Soller slit1 (º)	2.5	2θ increment (º)	0.02
Soller slit2 (º)	2.5	Crystal dist. scheme	Defect broadening
Sample length (cm)	4	Exchangeable cation	Ca^{2+}

Note: Mustar: mass absorption coefficient. RNDPWD: random powder option for calculating the Lorentz factor.

https://doi.org/10.1346/CCMN.2010.0580601 Published online by Cambridge University Press

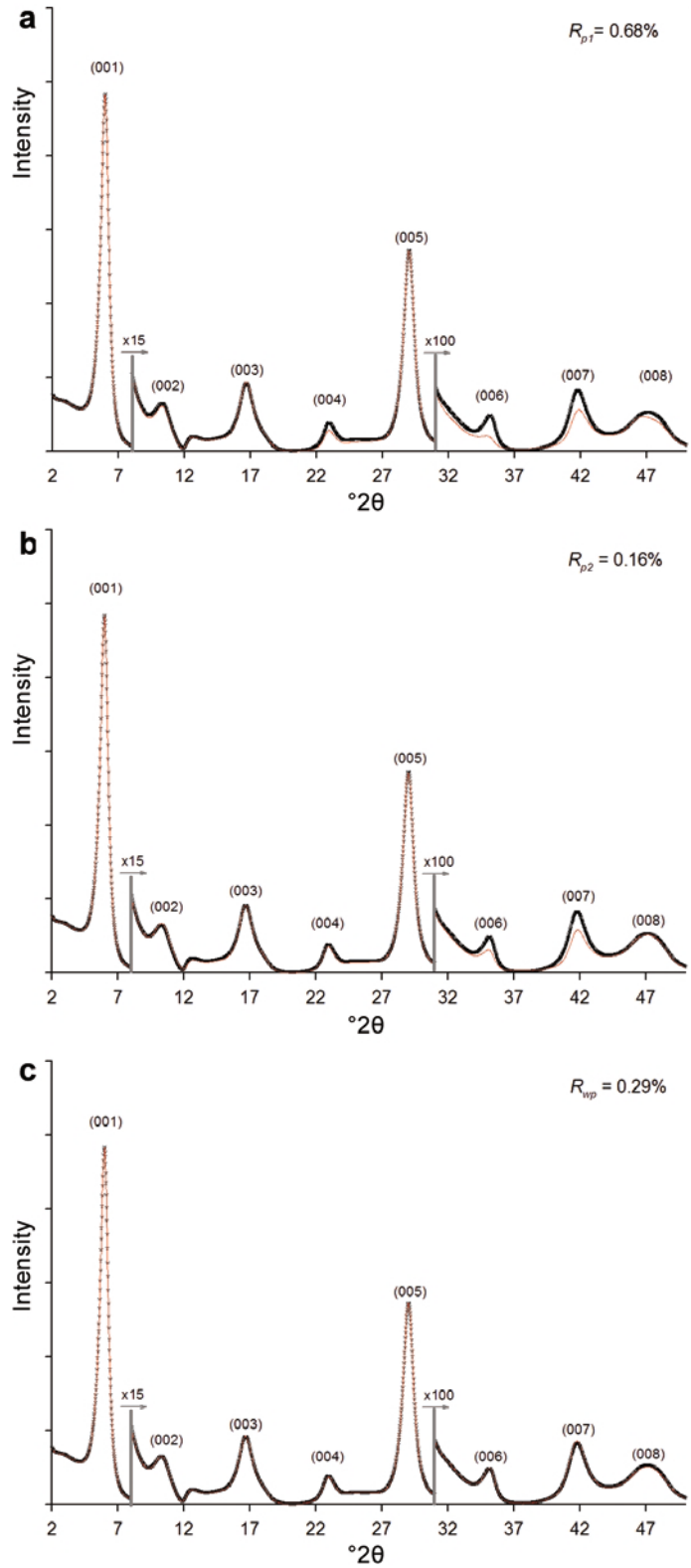


Figure 1. Fits to a simulated fitting target for interstratified 1W-2W smectite generated with NEWMOD+ using the parameters in Tables 1 and 2 using different fitting criteria, R_{p1}, R_{p2}, and R_{wp}. Black crosses represent the fitting target, and the curved line represents the fits to the simulated profile. Data are expanded by a factor of 15 above 8°2θ and by a factor of 100 above 31°2θ.

https://doi.org/10.1346/CCMN.2010.0580601 Published online by Cambridge University Press

Parameter accuracy in profile optimization is determined by parameter characteristics in the model, such as whether a parameter affects intensity, peak position, or both and whether a parameter is correlated with other parameters. Generally, the more a parameter influences intensity, the more accurate the refined parameter will be. This rule of thumb and the accuracy of each parameter (Table 1) provide insight into the choice of fitting parameters and help to evaluate the quality of refined parameters. The intensity contribution of the first-type disorder, ε_I, effectively acts as a thermal factor and is considerably smaller than the intensity contribution from the second-type disorder, ε_{II}, which acts as a strain effect. As a result, ε_I accuracies are generally less than ε_{II} accuracies (Table 1). Likewise, changes in interlayer-H_2O thermal factors, B_{1W} and B_{2W}, do not significantly affect overall intensities, although the consequences are evident at high diffraction angles. The two refined parameter values were less accurate, however. In addition, the cation-exchange capacity (CEC) or interlayer cation concentration (*i.e.* Ca^{2+}) is strongly correlated with C_{1W} and interlayer H_2O amounts in 1W smectite. This is based on the fact that both Ca^{2+} and H_2O are located at neighboring sites along the *Z* axis. The Ca^{2+} intensity contribution can be approximated by substituting the interlayer H_2O contribution or *vice versa*. For example, such correlations lead to lesser CEC- and C_{1W} -value accuracies of 66.5% and 92.4%, respectively, obtained using R_{wp}. Such correlations can be avoided or reduced by fixing the amounts of interlayer cations or by allowing cation amounts to vary between narrow limits, based on elemental compositions measured by an independent chemical method.

Fits to a synthetic profile for interstratified illite-smectite, I-S(EG)

A simulated profile for interstratified illite-smectite, I-S(EG), was generated using NEWMOD+ according to the values in Table 3 and the instrumental parameters in Table 2. Given the initial parameters shown in Table 3, the optimization routine driven by three fitting criteria yielded different 'best' fits, with R_{p1} = 0.26%, R_{p2} = 0.08%, and R_{wp} = 0.18%. Of the three 'best' fits shown in Figure 2, the weighted fitting scheme R_{wp} again produced the best visual fit compared with the two unweighted fitting schemes, R_{p1} and R_{p2}. The latter gave misfits in the region of the 008 reflection, a peak with relatively low intensity. In contrast to the fits to the synthetic profile of interstratified 1W-2W smectite, all three fits to the synthetic profile of I-S(EG) were of visually comparable quality. This may result from the presence of fewer parameter-correlation effects with the I-S(EG) optimization. Like the fits for the interstratified 1W-2W smectite, the fits for the I-S(EG) were all of high quality with very low *R* factors. Refined values of fitting parameters and boundary conditions for each fitting parameter are listed in Table 3, together with the accuracy of each parameter calculated according to equation 11. The CSD size for the synthesized I-S(EG) was assumed to follow a log-normal distribution (Środoń *et al.*, 1992; Eberl *et al.*, 1998), which can be described by:

$$N(x,\mu,\sigma) = \frac{1}{\sigma x\sqrt{2\pi}}\exp\left(-\frac{(\ln x-\mu)^2}{2\sigma^2}\right) \qquad (12)$$

where μ and σ represent the mean value and standard deviation, respectively, of ln *x*, where *x* is an individual

Table 3. Fitting parameters for interstratified I-S(EG).

Parameter	Target value	Initial value	LB	UB	R_{p1} Refined value	R_{p1} Accuracy	R_{p2} Refined value	R_{p2} Accuracy	R_{wp} Refined value	R_{wp} Accuracy
P(illite)	0.7	0.8	0.5	1	0.70	99.9	0.70	100.0	0.70	99.9
$d_{001(I)}$ (Å)	9.98	10	9.5	10.5	9.98	100.0	9.98	100.0	9.98	100.0
$\varepsilon_{I(I)}$	0.1	0.1	0	0.5	0.18	20.0	0.15	50.0	0.10	100.0
$\varepsilon_{II(I)}$	0.2	0.1	0	0.5	0.14	70.0	0.17	85.0	0.21	95.0
$Fe_{(I)}$	0.2	0.5	0	0.6	0.21	95.0	0.20	100.0	0.20	100.0
$K_{(I)}$	0.8	0.5	0.6	1	0.84	95.0	0.82	97.5	0.80	100.0
$d_{001(S)}$ (Å)	16.9	17.2	16.5	17.5	16.91	99.9	16.90	100.0	16.90	100.0
$\varepsilon_{I(S)}$	0.2	0.1	0	0.5	0.02	10.0	0.07	35.0	0.02	10.0
$\varepsilon_{II(S)}$	0.4	0.1	0	0.5	0.41	97.5	0.40	100.0	0.40	100.0
$Fe_{(S)}$	0.8	0.5	0	1.7	0.76	95.0	0.79	98.8	0.81	98.8
CEC	0.36	0.3	0.25	0.6	0.60	33.3	0.54	50.0	0.30	83.3
Reichweite	0.5	1	0	3	0.51	98.0	0.50	100.0	0.50	100.0
$\mu_{Lognormal}$	2	1	0.3	4	1.95	97.5	1.97	98.5	2.02	99.0
Sigmastar	10	12	0	30	9.34	93.4	9.67	96.7	10.07	99.3
High N	30	14	0	50	24	80.0	49	36.7	24	80.0
SF	1	3	0	1000	0.90	89.7	0.95	94.7	1.01	99.0

Conventions as in Table 1.

https://doi.org/10.1346/CCMN.2010.0580601 Published online by Cambridge University Press

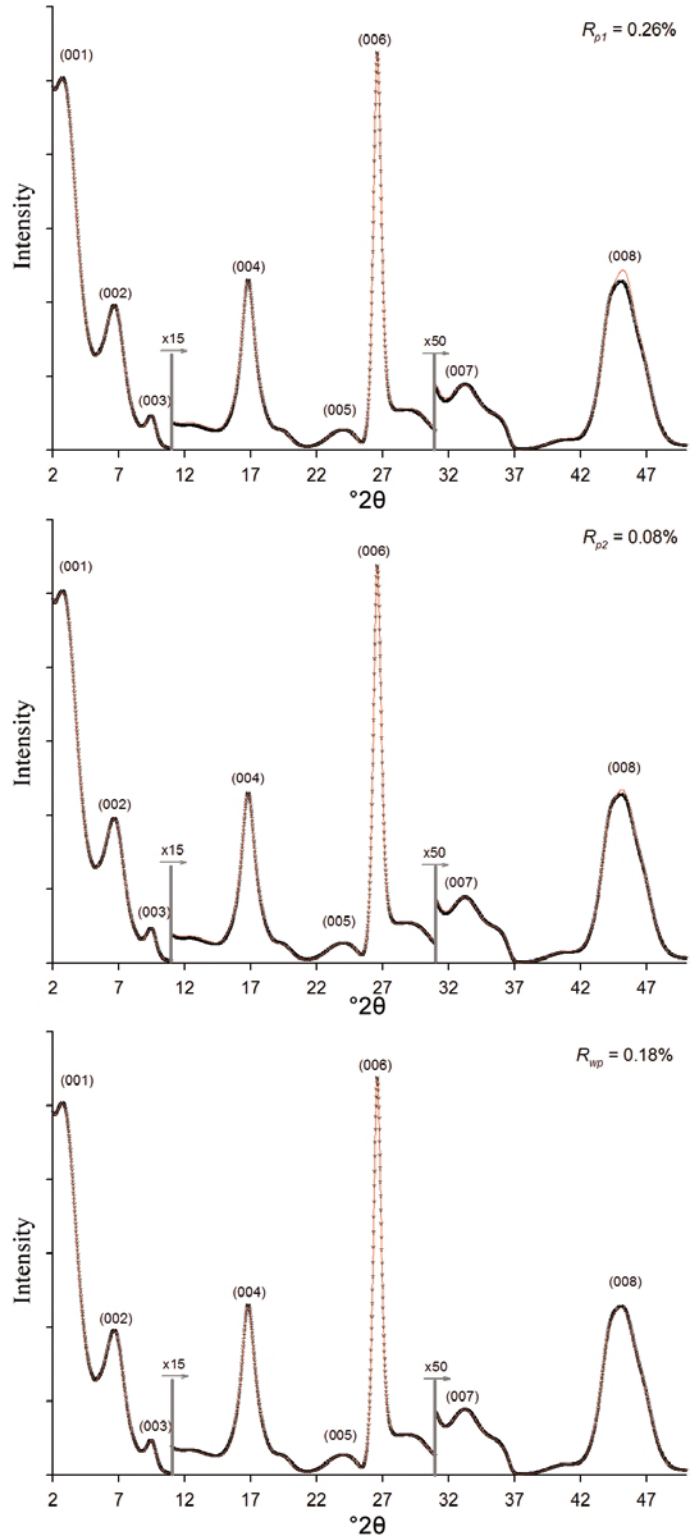


Figure 2. Fits to a simulated fitting target (I-S(EG)) generated using the parameters in Tables 2 and 3 based on three different fitting criteria. Conventions as in Figure 1. Black crosses represent the fitting target, and the curved line represents the fits to the measured profile. Data are expanded by a factor of 15 above 11°2θ and by a factor of 50 above 31°2θ.

https://doi.org/10.1346/CCMN.2010.0580601 Published online by Cambridge University Press

crystallite size. These two parameters can be further correlated through $\sigma^2 = 0.107\mu - 0.03$ (Środoń *et al.*, 2000), as they are strongly correlated in authigenic clay samples (Środoń *et al.*, 1992; Drits *et al.*, 1997b).

Fits to an experimental bi-hydrated smectite diffraction pattern

The configuration of interlayer species in bi-hydrated smectite, *i.e.* the concentration and position(s) of interlayer cations and H_2O molecules, has attracted particular interest recently (Ferrage *et al.*, 2005a, 2005b). Ferrage *et al.* (2005b) pointed out that the atomic positions and concentrations of interlayer H_2O molecules in bi-hydrated smectite (2W) given by Moore and Reynolds (1997) are incorrect. Their results suggested that significant discrepancies between experimental and simulated profiles for higher-order 00*l* reflections arise from the use of an incorrect structure model in which interlayer H_2O molecules are located at three distinct sites, 0.35 Å, 1.06 Å, and 1.20 Å along *Z*, with concentrations of 0.69, 0.69, and 1.4, respectively, per $O_{10}(OH)_2$. Ferrage *et al.* (2005b) proposed a new structure model based on molecular simulations in which interlayer H_2O molecules have a Gaussian distribution along the *Z* direction. In their model, the maximum electron density is located ~±1.2 Å away from the central interlayer cation, and the amount of interlayer H_2O molecules varies with relative humidity (r.h.). The model includes variations in the full-width at half-maximum (FWHM) and the Gaussian peak position of the electron density along the *Z* axis and in the concentration of interlayer H_2O molecules. In addition, Ferrage *et al.* (2005a, 2005b) assumed that the experimental diffraction profile is a combination of two interstratified systems with two or three components. They were able to reproduce experimental profiles measured under a wide range of relative humidities using this model and these assumptions. However, the assumption of a Gaussian distribution of interlayer H_2O molecules requires further investigation. First, their results showed that the basal spacing, d_{001}, of bi-hydrated smectite (2W) in Ca-SWy-1 (80% r.h.) is 15.51 Å, which leads to an interlayer region 5.51 Å thick, assuming a value of 10 Å for d_{001} of the collapsed Ca-SWy-1 (0W). According to Ferrage *et al.* (2005b), the interlayer H_2O Gaussian peak is located 1.37 Å from the mid-plane of the interlayer region, with a FWHM of 1.7 Å. These values give the interlayer H_2O density distribution shown in Figure 3 in which the density profile must drop to zero at the interlayer edges. The density peaks are significantly broader than the peaks derived from molecular simulation (figure 7 in Ferrage *et al.*, 2005b). Moreover, because the O^{2-} ionic radius in H_2O is 1.21 Å (Shannon, 1976), the interlayer region with H_2O should further decrease to the area designated by the two bold lines in Figure 3. This suggests that the Gaussian interlayer H_2O distribution defined by the values above is too large (this argument does not consider the possibility that H_2O molecules can partially penetrate the hexagonal rings). Second, the X-ray scattering factor for normally distributed (Gaussian) interlayer H_2O molecules can only be calculated by brute-force integration, which dramatically increases the calculation time required for profile fitting. In light of these limitations, a better approach is to describe the distribution of interlayer H_2O molecules using a conventional Debye-Waller thermal factor, *B*, commonly used in crystal structure refinements. Published values of *B* for H_2O in hydrated minerals, *e.g.* zeolites, can exceed 20 (*e.g.* Koyama and Takeuchi, 1977; Simoncic and Armbruster, 2004).

A series of XRD measurements was made on a Ca^{2+}-saturated SWy-1 smectite under controlled relative humidities at 23ºC using a BRUKER D8 diffractometer

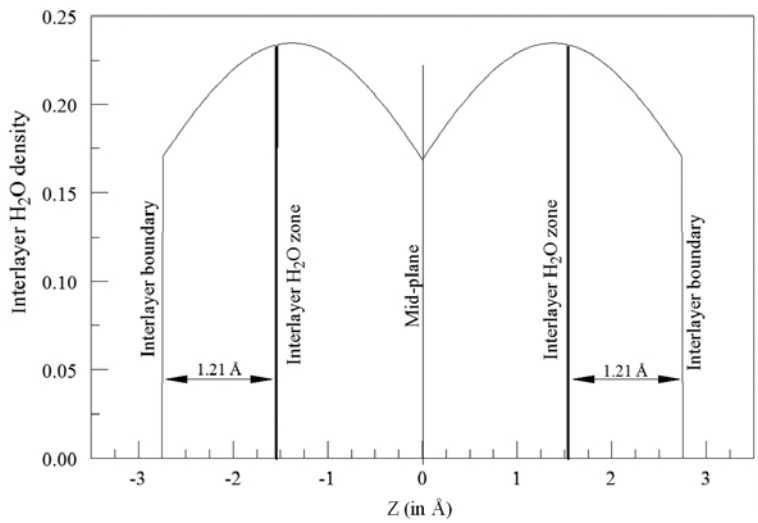


Figure 3. Density distribution of Ca-SWy-1 (80% r.h.) interlayer H_2O molecules according to Ferrage *et al.* (2005b). The "interlayer H_2O zone" is defined as the region between the two bold lines, which takes into account the radius of O^{2-}, 1.21 Å

https://doi.org/10.1346/CCMN.2010.0580601 Published online by Cambridge University Press

with 217.5 mm radius goniometer, a 1º divergence slit, two 2.4º Soller slits, and a sample length of 4 cm. Data were corrected for Lorentz-polarization effects prior to analysis. The basal spacing and FWHM of the 001 reflection at various humidities were obtained through peak fitting using the software package *TOPAS* (Coelho, 2003) with a split-Pearson VII (SP VII) profile function. The measured $FWHM_{001}$ was further corrected by multiplying by cosθ, where θ is the corresponding diffraction angle of the 001 peak (Drits *et al.*, 2005).

Measured $FWHM_{001}$ values plotted against relative humidity show a desorption-path minimum $FWHM_{001}$ of 0.371º2θ at 70% r.h. (Figure 4). For a given sample, $FWHM_{001}$ variation results primarily from changes in interstratified-component ordering as humidity changes, with only minor contribution from crystallite-size variation (Cases *et al.*, 1992). Therefore, the desorption-path interstratification effects were assumed to be at a minimum at 70% r.h., which resulted in a nearly pure bi-hydrate (2W). Thus, the 70% RH desorption profile was used to evaluate the optimization routine in FITMOD with particular attention to bi-hydrate smectite (2W) interlayer-H_2O configurations. Profile fitting for Ca-SWy-1 (70% r.h.) assumed interstratification of one- and two-layer H_2O montmorillonite phases (1W-2W). The fitting range was limited to 5−50º2θ due to significant experimental- and simulated-profile discrepancies at very low diffraction angles (<5º). During fitting, disorder of the first- and second-type for the two phases (*i.e.* ε_I and ε_{II}) and variables that describe interlayer H_2O configuration (*e.g.* concentration, position, and thermal factor, B) were allowed to vary, as well as other variables such as ordering and crystallite size. Minimizing R_{wp} (R_{wp} =10.92%) yielded the best fit and gave a 3.57% R_{p2} value assuming crystal-defect broadening. The larger R factors compared with fits to simulated profiles resulted from statistical noise in the experimental profiles and an imperfect model that may not fully represent observed profiles. Important parameter values yielded by the optimization routine and the boundary conditions used are listed in Table 4. The most significant differences between calculated and experimental profiles were in intensities and peak positions of the 003 reflection (Figure 5). In addition, the calculated 004 reflection intensity was greater than the experimental value. Ferrage *et al.* (2005b) discussed these misfits in detail and solved them for both reflections by introducing a third interstratified component (*i.e.* 0W, 1W, and 2W). Calculated higher-order reflections (006, 007, and 008) generally matched experimental profiles, with the 007 reflection only slightly offset to higher angles.

Minor misfit between the 006 and 007 and the 007 and 008 reflections (Figure 5) may be related to an additional interstratified phase (0W-1W-2W). This sample is dominantly (99%) a 2W smectite according to the fit results (Table 4). The basal spacings of the 1W and 2W components are 12.39 Å and 15.49 Å, respectively, which indicates interlayer spacings of 2.39 Å and 5.49 Å based on an assumed 10 Å dehydrated phase (0W). Given an O^{2-} radius of 1.21 Å (Shannon, 1976), interlayer H_2O molecules in 2W are more loosely packed along the Z direction than in 1W. This conclusion is supported by the 2W-component ε_I value of 0.39 Å and ε_{II} value of 0.44 Å. These values are greater than those for the 1W component, namely 0.23 Å and 0.36 Å. Loose packing of interlayer H_2O in 2W caused greater fluctuations in basal spacings than for 1W. The 3.36 $Å^2$ refined B value (thermal factor) for 1W is smaller than the 22.14 $Å^2$ value for 2W, consistent with the above arguments relating to interlayer H_2O packing. FITMOD yielded a refined interlayer-H_2O concentration (C_{2W}) of 4.32 H_2O per $O_{10}(OH)_2$. This is significantly larger than the Moore and Reynolds value

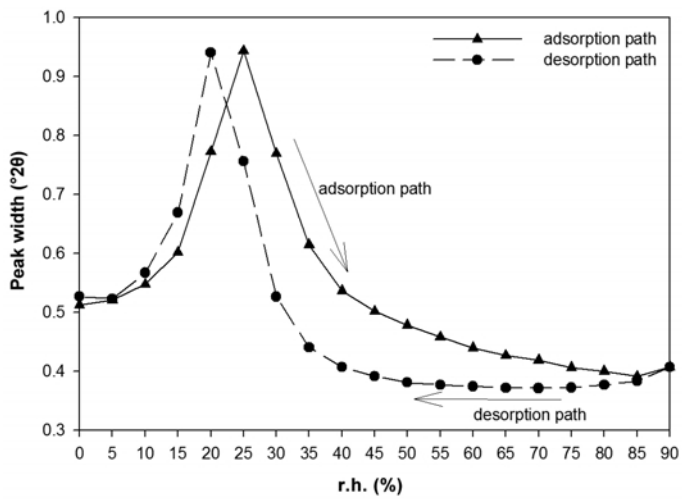


Figure 4. Relative humidity and d_{001} full-width at half-maximum ($FMHM_{001}$) of Ca-SWy-1 along an adsorption and desorption path.

https://doi.org/10.1346/CCMN.2010.0580601 Published online by Cambridge University Press

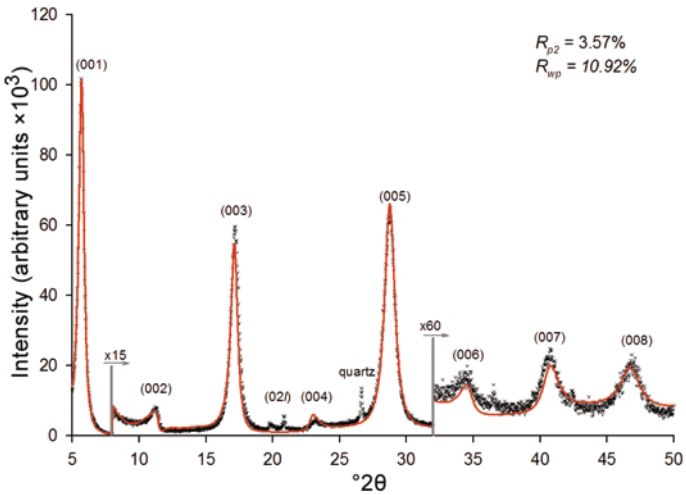


Figure 5. Fit to Ca-SWy-1 experimental profile measured at 70% r.h. on the desorption loop. Black crosses indicate the measured profile and the curved line is the optimized profile. Data were expanded by a factor of 15 above 8º2θ and by a factor of 60 above 32º2θ.

of 2.78 H_2O per $O_{10}(OH)_2$ but agrees with Ferrage *et al.* (2005b) values.

Fitting experimental XRD profiles of the I-S system

Experimental XRD patterns of interstratified illite-smectite, I-S(EG), samples were also used to test the profile-fitting algorithm in FITMOD. The XRD data for two purified I-S samples from Yucca Mountain drill cores, G1-4958 and G2-4873, were obtained using a Siemens D-500 diffractometer with a 1º divergence slit, two 2.4º Soller slits, and a sample length equal to 5 cm (Bish, 1989). These data were chosen for tests of FITMOD because results for the samples are published and the data were available. Sample G1-4958 was previously characterized as Reichweite = 1 with 60% illite layers and G2-4873 was characterized as Reichweite = 3 with 90% illite layers (Bish, 1989; Bish and Aronson, 1993). FITMOD minimized R_{wp}, and the CSD size was assumed to follow a log-normal distribution. The experimental data and optimized XRD patterns for two Yucca Mountain samples are plotted in Figures 6 and 7, and the fitting parameters, refined values, and boundary conditions are listed in Table 5. Good fits were obtained for the samples with R_{wp} values of 10.91% and 13.67% for samples G1-4958 and G2-4873, respectively, in reasonable agreement with previous results. The illite proportion for the G2-4873 sample was 0.85 and the Reichweite value was 2.53. Yuan and Bish (2010) used a traditional forward model in NEWMOD+ for G2-4873 and obtained an R_{p2} = 13.90% (figure 2 in Yuan and Bish, 2010), in contrast to R_{p2} = 9.47% for the current fit. They remarked that the misfit at ~8º, 17º, and 45º could be greatly reduced by decreasing the amount of K^+ in the illite component to an unrealistic value, 0.1 per $O_{10}(OH)_2$.They also observed the intensity contribution from the glass substrate at diffraction angles from ~12º2θ to 38º2θ, which suggests an insufficient sample thickness. The fit was improved by introducing the profile of the glass substrate as a background contribution. However, the intensities diffracted from a sample

Table 4. Fitting results for Ca-SWy-1 recorded at 70% r.h. on the desorption path.

Fitting parameter	Refined values	LB	UB	Fitting parameters	Refined values	LB	UB
$P_{(2W)}$	0.991	0.5	1	C_{1W}	2.33	1	2.5
$d_{001(2W)}$ (Å)	15.52	15.1	15.8	B_{1W} (Å^2)	3.36	0	25
$\varepsilon_{I(2W)}$	0.02	0	0.5	C_{2W}	4.31	2.5	6
$\varepsilon_{II(2W)}$	0.35	0	0.5	Δd_{wat}(Å)	1.47	1.1	1.6
$d_{001(1W)}$ (Å)	12.59	12.3	12.7	B_{2W} (Å^2)	21.14	0	25
$\varepsilon_{I(1W)}$	0.09	0	0.5	DFD	4.02	0	10
$\varepsilon_{II(1W)}$	0.17	0	0.5	High N	39	4	50
Fe	0.35	0	1.7	Reichweite	0.08	0	3
CEC	0.58	0.25	0.6				

Conventions as in Table 1.

https://doi.org/10.1346/CCMN.2010.0580601 Published online by Cambridge University Press

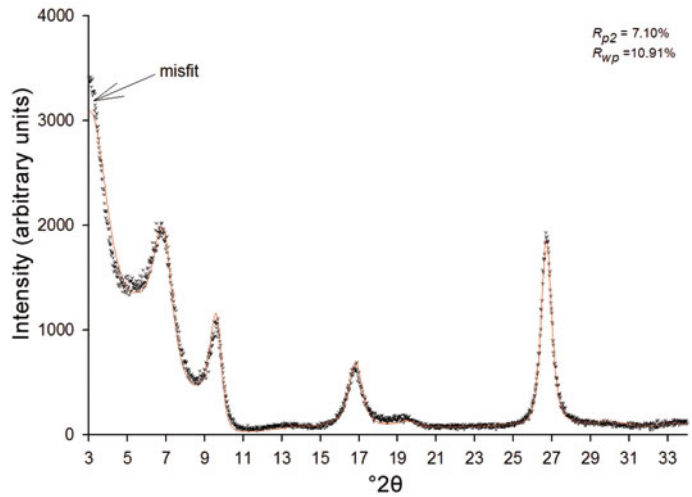


Figure 6. Experimental profile of I-S(EG) sample G1-4958 from Yucca Mountain, Nevada, fit using an assumed log-normal crystal-size distribution scheme.

with insufficient thickness must also be further corrected by equation 13, discussed in detail by Moore and Reynolds (equation 9.3, 1997):

$$\frac{I}{I_o} = \frac{\sin\theta}{2\mu^*}\left[1 - e^{\frac{-2\mu^* g}{\sin\theta}}\right] \quad (13)$$

where μ* is the mean sample-mass absorption coefficient and g is total mass of the sample, which is the product of sample density and sample thickness. With the introduction of disorder of the first- and second-type and, more importantly, the consideration of finite sample thickness, the discrepancies at ~8º, 17º, and 45º2θ were decreased significantly, leading to the smaller R_{p2} value compared with the fit reported previously. Although many studies have shown that the simulated profiles yielded by NEWMOD© exhibit significantly greater intensities at low diffraction angles compared with experimental profiles (Ferrage *et al.*, 2005a), good fits were obtained for both samples, particularly for sample G2-4873, in the low-angle region (<5º2θ). Further studies are required to investigate whether pattern misfit at low angles is caused by an inaccurate structural model, such as incorrect atomic positions or site occupancies, or by incorrect assumptions regarding the compositions of samples or perfect crystals *vs.* large particles with defects (Plançon, 2002), *etc.*

The accuracy of the profile-fitting optimization routine was demonstrated using both synthetic and experimental patterns, but the efficiency of the optimization process, *i.e.* the average time required for the optimization routine to achieve a reasonable fit, must also be considered. The average time required for optimization varies as a function of several factors,

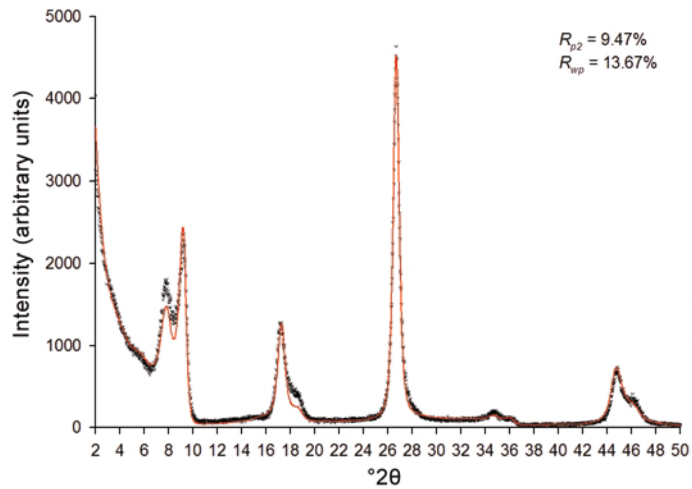


Figure 7. Experimental profile of I-S(EG) sample G2-4873 from Yucca Mountain, Nevada, fit using an assumed log-normal crystal-size distribution.

https://doi.org/10.1346/CCMN.2010.0580601 Published online by Cambridge University Press

Table 5. Fitting results for I-S samples G1-4958 and G2-4873 from Yucca Mountain, Nevada, USA.

Fitting parameter	LB	UB	G1-4958	G2-4873
$P(I)$	0.5	1	0.68	0.854
$d_{001(I)}$ (Å)	9.5	10.5	9.96	10.03
$\varepsilon_{I(I)}$	0	0.5	0.02	0.01
$\varepsilon_{II(I)}$	0	0.5	0.33	0.15
$Fe_{(I)}$	0	0.6	0.25	0.3
$K_{(I)}$	0.6	1	0.61	0.6
$d_{001(S)}$ (Å)	16.5	17.4	16.72	16.78
$\varepsilon_{I(S)}$	0	0.5	0.08	0.5
$\varepsilon_{II(S)}$	0	0.5	0.17	0.15
$Fe_{(S)}$	0	1.7	0.18	0.03
CEC	0.25	6	0.42	0.41
Sigmastar	0	30	2.93	3.49
$\mu_{log\text{-}normal}$	0.3	4	2.38	2.2
Reichweite	0	3	0.83	2.53
High N	4	50	32	35
Sample thickness (μm)	0	2000	13.46	9.63
Mustar (cm^2/g)	30	70	56.05	36.88

Conventions as in Tables 1 and 2.

including the number of data points (*i.e.* the 2θ range), the number of parameters varied in the fitting process, the computing power, and the number of perturbations (trials) applied in the optimization process. Statistical information showing the efficiency of the optimization routine during fitting of both the synthetic and experimental profiles examined above was tabulated (Table 6). The total time was recorded as processor time on a 3.0 GHz CPU for 10 perturbations. Experimental profiles exhibit more noise than synthetic profiles, and the model generally is unable to reproduce experimental profiles perfectly, leading to greater misfits in the optimized profiles with experimental data. This aspect of experimental patterns dramatically increases the number of required iterations and, therefore, increases the average time per perturbation from 2.4 min for fitting a synthetic profile to ~5 min. In practice, a good fit can be achieved with three or four perturbations. The optimization routine can be implemented with a multiple thread technique that allows distribution of the calculation load onto multiple central processing units, greatly reducing the profile-optimization time.

CONCLUSIONS

This paper describes, for the first time, the application of a reverse-modeling methodology for interpreting diffraction patterns from interstratified clay minerals. The program FITMOD used the downhill simplex method to fit XRD profiles by automatically varying all important structural and specimen parameters. The downhill simplex method has significant advantages over methods that rely on the function gradient, *e.g.* the Levenberg-Marquardt method, in both calculation time and the ability to adjust integer parameters. Compared with the GA methodology, the downhill simplex method converges (GA does not converge) and yields the optimal result more efficiently. As a result, the downhill simplex method is believed to be superior for fitting XRD profiles of interstratified phyllosilicates. However, most minimization techniques, including the downhill simplex method, have the potential to yield a minimum without knowing whether it is a global or a local minimum. FITMOD evaluates whether a minimum is global by perturbing the minimum with a slight change

Table 6. Efficiency of the optimization routine for various XRD profiles.

Fitting samples	Synthetic profiles		Experimental profiles		
	1W-2W	I-S(EG)	Ca-SWy-1 @ 70% r.h.	G1-4958	G2-4873
Number of variable parameters	19	16	22	20	20
Number of data points	2400	2400	2250	1600	2400
Number of iterations	36787	22240	46444	48184	43725
Number of perturbations	10	10	10	10	10
Total time (s)	1460	1429	3305	3255	2568
Average iterations/perturbation	3679	2224	4644	4818	4373
Average time/perturbation (min)	2.4	2.4	5.5	5.4	4.3

https://doi.org/10.1346/CCMN.2010.0580601 Published online by Cambridge University Press

in refined parameters, providing the ability to climb out of a local minimum. Based on the realistic outcomes of the fits shown here and experience with other systems, the downhill simplex method seems to efficiently avoid false minima. The existence of correlations among adjustable parameters has the potential to degrade the accuracy of fitting results and can lead to poor reproducibility in some cases, but this problem is common with all current fitting methods and can be minimized with judicious selection of refinable parameters and limits.

Three different unweighted and weighted fitting schemes were investigated with two sets of synthesized XRD profiles representing the interstratified 1W-2W and I-S(EG) systems, respectively, and R_{wp} consistently produced results which were superior to those obtained with the unweighted schemes, R_{p1} and R_{p2}. Thus, the R_{wp} scheme is favored for fitting experimental profiles.

FITMOD was applied to simulated and real data with excellent results, and results with simulated data provided excellent accuracy, even when starting parameters were far from the correct values. Application to previously published experimental data gave parameters and fits that appear superior to literature results. The methodology used in FITMOD can probably be extended to other simulation programs, such as WILDFIRE, which have similar difficulties with automatic parameter optimization.

REFERENCES

Bergmann, J., Kleeberg, R., and Taut, T. (1994) A new structure refinement and quantitative phase analysis method based on predetermined true peak profiles. *Zeitschrift für Kristallographie*, Supplement issue No. 8, European Crystallogrpahy Meeting **15**, Abstracts volume, p. 580.

Berkgaut, V., Singer, A., and Stahr, K. (1994) Palagonite reconsidered – paracrystalline illite-smectites from regoliths on basic pyroclastics. *Clays and Clay Minerals*, **42**, 582–592.

Bethke, C.M. and Reynolds, R.C. (1986) Recursive method for determining frequency factors in interstratified clay diffraction calculations. *Clay and Clay Minerals*, **34**, 224–226.

Bish, D.L. (1989) Evaluation of past and future alterations in tuff at Yucca Mountain, Nevada, based on the clay mineralogy of drill cores USW G-1, G-2, and G-3. *Los Alamos National Laboratory Report.* **LA-10667-MS**, 19–22.

Bish, D.L. and Aronson, J.L. (1993) Paleogeothermal and paleohydrologic conditions in silicic tuff from Yucca Mountain, Nevada. *Clays and Clay Minerals*, **41**, 148–161.

Casas-Cabanas, M., Palacin, M.R. and Rodriguez-Carvajal, J. (2005) Microstructural analysis of nickel hydroxide: Anisotropic size versus stacking faults. *Powder Diffraction*, **20**, 334–344.

Cases, J.M., Berend, I., Besson, G., Francois, M., Uriot, J.P., Thomas, F., and Poirier, J.E. (1992) Mechanism of adsorption and desorption of water-vapor by homoionic montmorillonite.1. The sodium-exchanged form. *Langmuir*, **8**, 2730–2739.

Coelho, A.A. (2003) *TOPAS*. User Manual. Version 3.1. Bruker AXS GmbH, Karlsruhe, Germany.

Cuadros, J. and Dudek, T. (2006) FTIR investigation of the evolution of the octahedral sheet of kaolinite-smectite with progressive kaolinization. *Clays and Clay Minerals*, **54**, 1–11.

David, W.I.F. (2004) Powder diffraction: Least-squares and beyond. *Journal of Research of the National Institute of Standards and Technology*, **109**, 107–123.

de la Fuente, S., Cuadros, J., and Linares, J. (2002) Early stages of volcanic tuff alteration in hydrothermal experiments: Formation of mixed-layer illite-smectite. *Clays and Clay Minerals*, **50**, 578–590.

Drits, V.A. and Sakharov, B.A. (1976) *X-ray Analysis of Mixed-layer Clay Minerals*. Nauka, Moscow, 256 pp. (in Russian).

Drits, V.A. and Tchoubar, C. (1990) *X-ray Diffraction by Disordered Lamellar Structures*. Springer Verlag, Berlin, Heidelberg, 371 pp.

Drits, V.A., Sakharov, B.A., Lindgreen, H. and Salyn, A. (1997a) Sequential structure transformation of illite-smectite-vermiculite during diagenesis of Upper Jurassic shales from the North Sea and Denmark. *Clay Minerals*, **32**, 351–371.

Drits, V., Środoń, J. and Eberl, D.D. (1997b) XRD measurement of mean crystalline thickness of illite and illite/smectite: Reappraisal of the Kubler index and the Scherrer equation. *Clays and Clay Minerals*, **45**, 461–475.

Drits, V.A., Sakharov, B.A., Dainyak, L.G., Salyn, A.L., and Lindgreen, H. (2002) Structural and chemical heterogeneity of illite-smectites from Upper Jurassic mudstones of East Greenland related to volcanic and weathered parent rocks. *American Mineralogist*, **87**, 1590–1606.

Drits, V.A., Sakharov, B.A., Salyn, A.L., and Lindgreen, H. (2005) Determination of the content and distribution of xed ammonium in illite-smectite using a modied X-ray diffraction technique: Application to oil source rocks of western Greenland. *American Mineralogist*, **90**, 71–84.

Dudek, T., Cuadros, J., and Fiore, S. (2006) Interstratified kaolinite-smectite: Nature of the layers and mechanism of smectite kaolinization. *American Mineralogist*, **91**, 159–170.

Eberl, D.D., Nuesch, R., Šucha, V., and Tsipursky, S. (1998) Measurement of fundamental illite particle thicknesses by X-ray diffraction using PVP-10 intercalation. *Clays and Clay Minerals*, **46**, 89–97.

Ferrage, E., Lanson, B., Sakharov, B.A., and Drits, V.A. (2005a) Investigation of smectite hydration properties by modeling experimental X-ray diffraction patterns: Part I. Montmorillonite hydration properties. *American Mineralogist*, **90**, 1358–1374.

Ferrage, E., Lanson, B., Malikova, N., Plançon, A., Sakharov, B.A. and Drits, V.A. (2005b) New insights on the distribution of interlayer water in bi-hydrated smectite from X-ray diffraction profile modeling of 00l reflections. *Chemistry of Materials*, **17**, 3499–3512.

Gruner, J.W. (1934) The structure of vermiculites and their collapse by dehydration. *American Mineralogist*, **19**, 557–575.

Gualtieri, A.F., Ferrari, S., Leoni, M., Grathoff, G., Hugo, R., Shatnawi, M., Paglia, G., and Billinge, S. (2008) Structural characterization of the clay mineral illite-1M. *Journal of Applied Crystallography*, **41**, 402–415.

Guinier, A. (1964) Théorie et technique de la radiocristallographie. Pp. 490–636 in: *Diffraction par les Réseaux Cristallins Imparfaits*. Dunod, Paris.

Hendricks, S.B. and Teller, E. (1942) X-ray interference in partially ordered layer lattices. *Journal of Chemical Physics*, **10**, 147–167.

Hillier, S. and Velde, B. (1992) Chlorite interstratified with a 7-Å mineral – An example from offshore Norway and possible implications for the interpretation of the composi-

https://doi.org/10.1346/CCMN.2010.0580601 Published online by Cambridge University Press

tion of diagenetic chlorites. *Clay Minerals*, **27**, 475–486.
Howard, S.A. and Preston, K.D. (1989) Profile fitting of powder diffraction patterns. Pp. 217–275 in: *Modern Powder Diffraction* (D.L. Bish and J.E. Post, editors). Reviews in Mineralogy, **20**, Mineralogical Society of America, Washington, D.C.
Howard, S.A. and Snyder, R.L. (1983) An evaluation of some profile models and the optimization procedures used in profile fitting. *Advances in X-ray Analysis*, **26**, 73–81.
Jaboyedoff, M. and Cosca, M.A. (1999) Dating incipient metamorphism using Ar^{40}/Ar^{39} geochronology and XRD modeling: a case study from the Swiss Alps. *Contributions to Mineralogy and Petrology*, **135**, 93–113.
Jaboyedoff, M. and Thelin, P. (1996) New data on low-grade metamorphism in the Brianconnais domain of the Prealps, Western Switzerland. *European Journal of Mineralogy*, **8**, 577–592.
Koyama, K. and Takeuchi, Y. (1977) Clinoptilolite – distribution of potassium atoms and its role in thermal stability. *Zeitschrift fur Kristallographie*, **145**, 216–239.
Leoni, M., Gualtieri, A.F., and Roveri, N. (2004) Simultaneous refinement of structure and microstructure of layered materials. *Journal of Applied Crystallography*, **37**, 166–173.
MacEwan, D.M.D. (1958) Fourier transform methods for studying X-ray scattering from lamellar systems. II. The calculation of X-ray diffraction effects from various type of interstratification. *Kolloidzeitschrift*, **156**, 61–67.
MacEwan, D.M.C., Ruiz-Amil, A. and Brown, G. (1961) Interstratified clay minerals. Pp. 393 in: *The X-ray Identification and Crystal Structures of Clay Minerals* (G.W. Brindley and G. Brown, editors). The Mineralogical Society, London.
Marquardt, D.W. (1963) An algorithm for least-squares estimation of nonlinear parameters. *Journal of the Society for Industrial and Applied Mathematics*, **11**, 431–441.
Méring, J. (1949) X-ray diffraction in disordered layer structures. *Acta Crystallographica*, **2**, 371–377.
Moore, D.M. and Reynolds, R.C., Jr. (1997) *X-ray Diffraction and the Identification and Analysis of Clay Minerals*. Oxford University Press, New York, 369 pp.
Nelder, J.A. and Mead, R. (1965) A simplex method for function minimization. *Computer Journal*, **7**, 308–313.
Pevear, D.R. and Schuette, J.F. (1993) Inverting the NEWMOD X-ray diffraction forward model for clay minerals using genetic algorithms. Pp. 20–41 in: *Computer Applications to X-ray Powder Diffraction Analysis of Clay Minerals* (R.C. Reynolds Jr. and J.R. Walker, editors). CMS Workshop Lectures, Vol. **5**, The Clay Minerals Society, Boulder, Colorado, USA.
Plançon, A. (1981) Diffraction by layer structures containing different kinds of layers and stacking-faults. *Journal of Applied Crystallography*, **14**, 300–304.
Plançon, A. (2002) New modeling of X-ray diffraction by disordered lamellar structures, such as phyllosilicates. *American Mineralogist*, **87**, 1672–1677.
Press, W.H., Teukolsky, S.A., Vetterling, W.T. and Flannery, B.P. (1992) *Numerical recipes in C: The Art of Scientific Computing*, 2nd edition. Cambridge University Press, Cambridge, UK.
Proffen, T. and Neder, R.B. (1997) DISCUS: A program for diffuse scattering and defect-structure simulation. *Journal of Applied Crystallography*, **30**, 171–175.
Renac, C. and Meunier, A. (1995) Reconstruction of palaeothermal conditions in a passive margin using illite-smectite mixed-layer series (Ba1 Scientific Deep Drill-Hole, Ardeche, France). *Clay Minerals*, **30**, 107–118.
Reynolds, R.C. (1967) Interstratified clay systems: Calculation of the total one-dimensional diffraction function. *American Mineralogist*, **52**, 661–672.
Reynolds, R.C. (1980) Interstratified clay minerals: Pp. 249–303 in: *Crystal Structures of Clay Minerals and their X-ray Identification* (G.W. Brindley and G. Brown, editors). Mineralogical Society, London.
Reynolds, R.C., Jr. (1985) NEWMOD, *a Computer Program for the Calculation of Basal X-Ray Diffraction Intensities of Mixed-Layered Clays*. R.C. Reynolds, Hanover, New Hampshire, 03755, USA.
Reynolds, R.C., Jr. (1989) Diffraction by small and disordered crystals. Pp. 143–182 in: *Modern Powder Diffraction* (D.L. Bish and J.E. Post, editors). Reviews in Mineralogy, **20**, Mineralogical Society of America, Washington, D.C.
Schreyer, W., Medenbach, O., Abraham, K., Gebert, W., and Muller, W.F. (1982) Kulkeite, a new metamorphic phyllosilicate mineral – ordered 1-1 chlorite talc mixed-layer. *Contributions to Mineralogy and Petrology*, **80**, 103–109.
Shannon, R.D. (1976) Revised effective ionic-radii and systematic studies of interatomic distances in halides and chalcogenides. *Acta Crystallographica Section A*, **32**, 751–767.
Simoncic, P. and Armbruster, T. (2004) Peculiarity and defect structure of the natural and synthetic zeolite mordenite: a single-crystal X-ray study. *American Mineralogist*, **89**, 421–431.
Środoń, J., Elsass, F., McHardy, W.J., and Morgan, D.J. (1992) Chemistry of illite-smectite inferred from TEM measurements of fundamental particles. *Clay Minerals*, **27**, 137–158.
Środoń, J., Eberl, D.D., and Drits, V.A. (2000) Evolution of fundamental-particle size during illitization of smectite and implications for reaction mechanism. *Clays and Clay Minerals*, **48**, 446–458.
Toby, B.H. (2006) R factors in Rietveld analysis: How good is good enough? *Powder Diffraction*, **21**, 67–70.
Treacy, M.M.J., Newsam, J.M., and Deem, M.W. (1991) A general recursion method for calculating diffracted intensities from crystals containing planar faults. *Proceedings of the Royal Society of London, A: Mathematical and Physical Sciences*, **433**, 499–520.
Ufer, K., Kleeberg, R., Bergmann, J., Curtius, H., and Dohrmann, R. (2008) Refining real structure parameters of disordered layer structures within the Rietveld method. *Zeitschrift fur Kristallographie*, 151–158.
Walker, J.R. (1993) An introduction to computer modeling of X-ray diffraction patterns of clay minerals: A guided tour of NEWMOD. Pp. 1–18 in: *Computer Applications to X-ray Powder Diffraction Analysis of Clay Minerals* (R.C. Reynolds Jr. and J.R. Walker, editors). CMS Workshop Lectures series, vol. **5**, The Clay Minerals Society, Boulder, Colorado, USA.
Wilson, P.N., Parry, W.T. and Nash, W.P. (1992) Characterization of hydrothermal tobelitic veins from black shale, Oquirrh Mountains, Utah. *Clays and Clay Minerals*, **40**, 405–420.
Yuan, H.J. and Bish, D.L. (2010) NEWMOD+, a new version of the NEWMOD program for interpreting X-ray powder diffraction patterns from interstratified clay minerals. *Clays and Clay Minerals*, **58**, 318–326.
Young, R.A. (1993) Introduction to the Rietveld method. Pp. 1–38 in: *The Rietveld Method* (R.A. Young, editor). International Union of Crystallography, Oxford University Press. Oxford, UK.

(*Received 19 February 2010; revised 21 October 2010; Ms. 414; A.E. J.W. Stucki*)

https://doi.org/10.1346/CCMN.2010.0580601 Published online by Cambridge University Press